Contents

Contributors

Klaus Schulten *Department of Physics, University of Illinois at Urbana-Champaign, and Beckman Institute for Advanced Science and Technology, Urbana-Champaign, Illinois, USA*

Shigehiko Hayashi *Department of Chemistry, Graduate School of Sciences, Kyoto University, Kyoto, Japan*

11

Quantum Biology of Retinal

Klaus Schulten,[a] Shigehiko Hayashi,[b]

11.1 Introduction

Retinal is a biological chromophore ubiquitous in visual receptors of higher life forms, but serving also as an antenna in light energy transformation and phototaxis of bacteria. The chromophore arises in various retinal proteins, the best known two being the visual receptor rhodopsin and the light-driven proton pump bacteriorhodopsin. The ubiquitous nature of retinal in photobiology is most remarkable as the molecule shows an extremely wide adaptability of its spectral absorption characteristics and a precise selection of its photoproducts, both properties steered by retinal proteins.

Rhodopsin (Rh) is a membrane protein of the rod cells in the retina of animal eyes and contains a retinal molecule as a chromophore surrounded by the protein's seven transmembrane helices (Khorana, 1992) as shown in Fig. 11.1. Rh serves as the receptor protein for monochromic vision, in particular, for vision in the dark. Analogous retinal proteins, called iodopsins, exist in the cone cells of the retina and serve as receptor proteins for color vision in day light (Nathans et al., 1986).

Retinal proteins serve also in certain bacteria as light-driven proton pumps that maintain the cell potential as in case of bacteriorhodopsin (bR) (Schulten and Tavan, 1978), or as light sensors in bacterial phototaxis (Spudich and Jung, 2005).

All retinal proteins are structurally homologous, being composed of seven transmembrane helices with a retinal chromophore bound to a lysine side group. The photoactivation mechanisms of the proteins' retinal moieties are similar, but distinct from each other. The primary event of retinal photoactivation is a photoisomerization reaction (Birge, 1990). The photobiological

[a] E-mail: kschulte@ks.uiuc.edu, Supported by NIH P41-RR005969, NSF MCB-0744057 and NSF PHY0822613
[b] E-mail: hayashig@kuchem.kyoto-u.ac.jp

mechanism of retinal has been fascinating experimental and theoretical researchers over many decades until today. In this chapter, the quantum processes involved in the photoactivation of retinal in Rh and related proteins are presented.

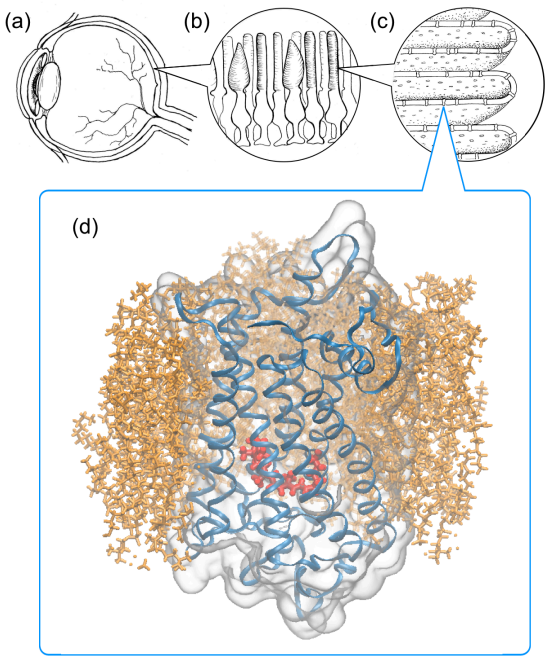

Figure 11.1 Visual receptors. (a) Cross section of the eye with lens and iris on the left and the retina with nerve cells highlighted on the right. (b) The retinas of animals contain millions of rod and cone receptor cells. Shown are shapes and arrangement of rod and cone cells. (c) Discs in the cone and rod cells. The discs are hollow and made of membranes that are saturated with the light receptor protein, rhodopsin (Rh), in case of rods, and several types of proteins, iodopsins, in case of cones. In the figure Rhs are highlighted. (d) Light is absorbed by retinal (red), the chromatophore molecule situated inside Rh (blue tube and grey surface), which in turn is located inside a lipid (brown) membrane. Light excited retinal undergoes an isomerization reaction triggering the visual signal; this chapter describes the quantum mechanical nature of retinal's light absorption characteristics and photo reactions.

11.2 Retinal in Rhodopsin and Bacteriorhodopsin

Figure 11.2 depicts the chemical structure of the retinal chromophore, mainly a polyene chain with six conjugated double bonds. One end of the polyene

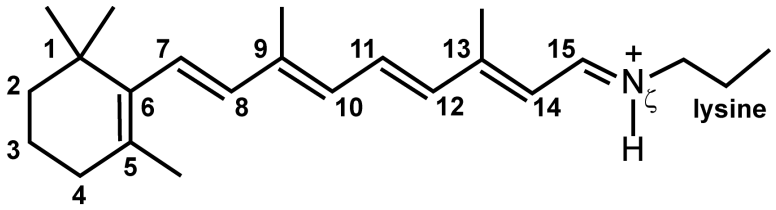

Figure 11.2 Chemical structure of the retinal chromophore linked through a protonated Schiff base to a lysine amino acid residue of the sensory protein rhodopsin; the nitrogen atom involved in the linkage is protonated. The polyene backbone of retinal ends on the right side in the protonated Schiff base and on the left side in a β-ionone ring. Shown is the conventional numbering of retinal carbon atoms. Bonds depicted by two parallel lines, e.g., the 11-12 bond, are the so-called double bonds that exhibit typically very high (compared to physiological thermal energy $k_{\mathrm{B}}T$) torsional energy barriers preventing spontaneous $0^o \rightarrow 180^o$ rotation; bonds depicted by a single line, e.g., the 1–11 bond, are the so-called single bonds that exhibit typically lower torsional energy barriers.

chain is covalently attached to a lysine residue through a protonated Schiff base (PSB); the other end forms a β-ionone ring. Upon photoabsorption, the polyene part of retinal undergoes isomerization towards an isomer different from that of the initial (reactant) state, i.e., one of retinal double bonds (discussed further below) rotates by 180^o. During the primary, extremely fast (50 - 500 fs) isomerization step, retinal, confined to its tight protein binding pocket, is forced to accommodate the 180^o rotation around one bond with a minimal change of its overall shape, which it achieves through torsional counter-rotations involving its other bonds, though in doing so ending up in a high energy conformation. Due to the high energy content, the torsional distortions of retinal seek to relax, which brings about an overall shape change of retinal that can be accommodated only if the surrounding protein alters its shape, too. This accommodation and subsequent protein processes coupled to it, for example motion of internal water and proton transfer, initiates a photocycle during which the retinal protein assumes a new functional state.

In case of Rh, the protein enters an intermediate signaling state that activates a cascade of signaling reactions involving other proteins. Eventually, the cascade amplifies Rh signaling sufficiently that the interior electrical potential of the rod cell changes enough to induce firing of neurons, the so-called ganglion cells, linking the retina to a brain area relevant for vision. The description given here does not do justice to the complexity and impressive function of the retina.

In case of bR, the changes in the protein interior brought about by retinal photoisomerization induce the vectorial transfer of a proton from the interior to the exterior of the bacterial cell wall, in which bR resides, charging the bacterial cell energetically.

As shown in Fig. 11.1, Rh is a visual pigment responsible in animal eyes for monochromic vision in the dark. In the human eye, three other visual pigments, iodopsins, also exist in the retina, namely in the so-called cone cells, and are responsible for color vision. The visual pigments are members of the protein family of G-protein coupled receptors (GPCRs); photoactivation of the receptors leads to binding of G-protein to initiate a signaling transduction cascade (Shichida and Imai, 1998). Figures 11.1d, 11.3a depict the protein structure of Rh. In the resting dark state of Rh and the three human iodopsins, retinal is found in an 11-cis configuration. The primary photoreaction is a photoisomerization of retinal from its 11-cis state to its all-trans state as shown in Fig. 11.3b. The photoisomerization reaction in Rh is one of the fastest molecular reactions in nature; it completes within 200 fs (Kochendoerfer and Mathies, 1996; Polli et al., 2010; Schoenlein et al., 1991).

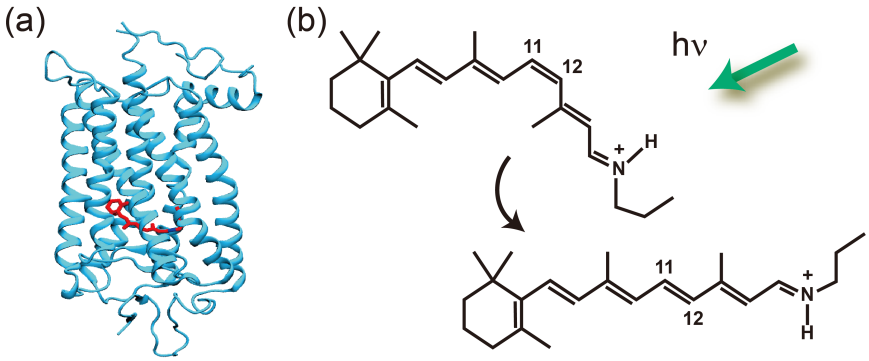

Figure 11.3 (a) Structure and photodynamics of rhodopsin. Seven transmembrane helices of the protein embed a retinal (red). (b) Photoreaction in Rh. Upon photoabsorption, retinal undergoes isomerization from 11-cis to all-trans. Retinal is shown bound as a protonated Schiff base to a lysine residue.

Photoabsorption spectra of Rh and of the three iodopsins reach over a wide range of the visible spectrum: the photoabsorption maximum of Rh is at 500 nm, i.e., at a wavelength where sun light has maximum intensity on the surface of Earth. Photoabsorption of the three human iodopsins covers 400-500 nm, 450-630 nm, and 500-700 nm with absorption maxima around 430, 550, and 570 nm. The absorption characteristics permit the iodopsins to

discriminate color hues, an impressive ability as most readers can judge. It is remarkable that all four human visual receptors employ 11-cis retinal, yet absorb 400-700 nm light; the quantum mechanical mechanism underlying spectral tuning is explained further below.

Microbial rhodopsins are widely distributed in archaea, bacteria, and unicellular eukaryotes, and function as photosynthetic light-driven ion pumps and photosensory receptors (Spudich and Jung, 2005). The proteins exhibit high sequence homology with one another, but no detectable homology with GPCR rhodopsins is seen. Recently, microbial rhodopsins have attracted much attention for their wide distribution in the huge euphotic zone of the deep sea (Beja et al., 2000; Kolber et al., 2000). Microbial rhodopsins also caught the limelight as tools of a newly developed neuroscience technique called optogenetics; neural circuits are controlled in vivo by photoillumination through photosensitive ion channel and pump rhodopsins genetically expressed in neurons (Zhang et al., 2007).

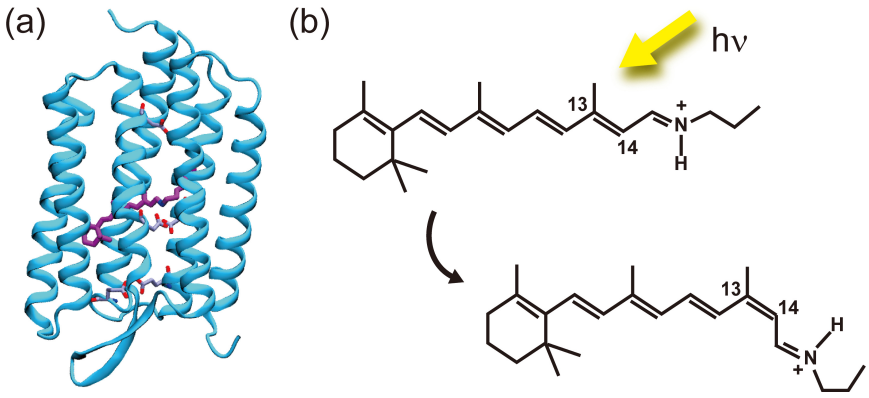

Figure 11.4 (a) Structure and photodynamics of bacteriorhodopsin. A PSB retinal chromophore (purple) is located in the protein. Carboxylate protein groups in the proton channel, involved in light-induced proton pumping, are also highlighted. (b) Photoreaction in bR. Upon photoabsorption, retinal undergoes an all-trans to 13-cis isomerization.

Bacteriorhodopsin (bR), an extensively studied archaeal rhodopsin, functions as a light driven proton pump. Figure 11.4a depicts the structure of bR. A proton channel exists in the region between the transmembrane helices, involving carboxylate side-chain groups, the protonated Schiff base of retinal and water molecules. In the dark resting state of bR, retinal is found in its all-trans form, i.e., not in its 11-cis form as in the visual receptors. The primary photoreaction isomerizes the all-trans form to the 13-cis one as

shown in Fig. 11.4b. The photoisomerization reaction in bR, as in Rh, is fast with a sub-picosecond time constant (Gai et al., 1998). The photoisomerization triggers a photocycle that couples protein conformational changes to vectorial proton transport from the cytoplasmic side to the extracellular side of the bacterial cell membrane.

As in the case of visual receptors, absorption spectra of microbial rhodopsins are adapted to the bacterial habitat and to their particular function. For example, the spectra of protorhodopsin of various aquatic species are adapted to the water depth in which a species typically lives. Another example is furnished by bacterial rhodopsins, sRI and sRII, which function as sensors for phototaxis in archaebacteria and possess different photoabsorption spectra due to their opposite functions. The absorption maximum of sRI, 587 nm, is close to the maxima of bacterial rhodopsins acting as ion pumps serving cell function and, thus, sRI features positive phototaxis guiding the bacteria to the suitable light environment. sRII, however, with an absorption maximum at 498 nm, features negative phototaxis and, mainly expressed in an aerobic environment situation, repels bacteria from the intense light at $\sim$500 nm typical for such environments; sRII, thereby, prevents photooxydative damage to the cells.

11.3 Quantum Physics of Excited State Dynamics

An electronically excited state of the chromophore generated by absorption of a photon decays one way or other to the electronic ground state. In a photoactive protein the decay route is controlled depending on the protein's function, favoring a route that ends up in a new energy minimum on the ground state surface; in this minimum the protein is in its active state. Here we outline the quantum mechanical description of the excited state dynamics and its control.

The excited state processes involve the nuclear motion of chromatophore and protein proceeding on the *Born-Oppenheimer (BO) or adiabatic* potential energy surfaces of the excited and ground electronic states and involve also transition between the two surfaces. The description of the processes is based on the non-relativistic Hamiltonian of the system, $\hat{H}$, that is expressed as a differential operator with respect to coordinates of electrons, $\mathbf{r}$, and coordinates of nuclei, $\mathbf{R}$,

$$\hat{H}(\mathbf{r},\mathbf{R}) = \hat{T}_N(\mathbf{R}) + \hat{H}_{BO}(\mathbf{r},\mathbf{R}) \quad . \tag{11.1}$$

Here $\hat{T}_N(\mathbf{R})$ is the nuclear kinetic energy operator and $\hat{H}_{BO}(\mathbf{r},\mathbf{R})$ is the BO Hamiltonian, which consists of the electronic Hamiltonian and the nuclear

repulsion energy

$$\hat{H}_{BO}(\mathbf{r},\mathbf{R}) = \sum_{i}^{N_{elec}} \left(-\frac{\hbar^2}{2m_e}\nabla_i^2 \right) - \sum_{i}^{N_{elec}} \sum_{A}^{N_{nuc}} \frac{Z_A e^2}{4\pi\epsilon_0 r_{iA}} + \sum_{i}^{N_{elec}} \sum_{j>i}^{N_{elec}} \frac{e^2}{4\pi\epsilon_0 r_{ij}} + \sum_{A}^{N_{nuc}} \sum_{B>A}^{N_{nuc}} \frac{Z_A Z_B e^2}{4\pi\epsilon_0 R_{AB}} \quad , \tag{11.2}$$

where N_{elec} and N_{nuc} are the number of electrons and nuclei, respectively, m_e is the mass of the electron, $\hbar = h/(2\pi)$ is the reduced Planck constant, Z_A is the atomic number of atom A, e is the elementary electric charge, and ϵ_0 is the vacuum permittivity. Electronic and nuclear motion are separated according to the *Born-Oppenheimer (BO) approximation*. In this approximation electronic wavefunction and energy of the electronic states are determined by solving the Schrödinger equation for $\hat{H}_{BO}(\mathbf{r},\mathbf{R})$:

$$\hat{H}_{BO}(\mathbf{r},\mathbf{R})\Psi_I(\mathbf{r},\mathbf{R}) = E_I^{BO}(\mathbf{R})\Psi_I(\mathbf{r},\mathbf{R}) \quad , \tag{11.3}$$

where $\Psi_I(\mathbf{r},\mathbf{R})$ and $E_I^{BO}(\mathbf{R})$ are the BO or adiabatic wave function and energy, respectively, of the I-th electronic state at a fixed nuclear geometry $\mathbf{R}$. The eigenvalue problem (11.3) is solved through methods of quantum chemistry.

In general, the excited state decay involves more than one decay path; the paths compete with each other kinetically (Atkins and de Paula, 2009). Figure 11.5 depicts schematically possible paths. First, upon *photoabsorption,* the chromophore in the resting electronic ground state is promoted to the electronic excited state, according to the Franck-Condon (FC) principle without changing the nuclear geometry, in what is referred to as a *vertical excitation*. The conformational space region in the excited state reached after the vertical excitation from the ground state nuclear Boltzmann distribution is called the *FC region*. The FC region is usually not at an energy minimum of the excited state potential energy surface and, hence, the vertical excitation generates vibrationally excited (i.e., hot) states of nuclear motion, which relax immediately, dissipating their energy into surrounding nuclear degrees of freedom and effectively cooling the nuclear motion viewed along nuclear coordinates involved in further key geometrical changes.

One of the main decay paths after photoexcitation is *fluorescence* where the chromophore decays "vertically" back to the electronic ground state by emitting a photon, the wave length of which corresponds to the energy gap bridged in the vertical decay. Other decay paths involve *non-radiative transitions* in which the system moves to a nuclear geometry, where excited state and ground state energy surfaces intersect, and transitions to

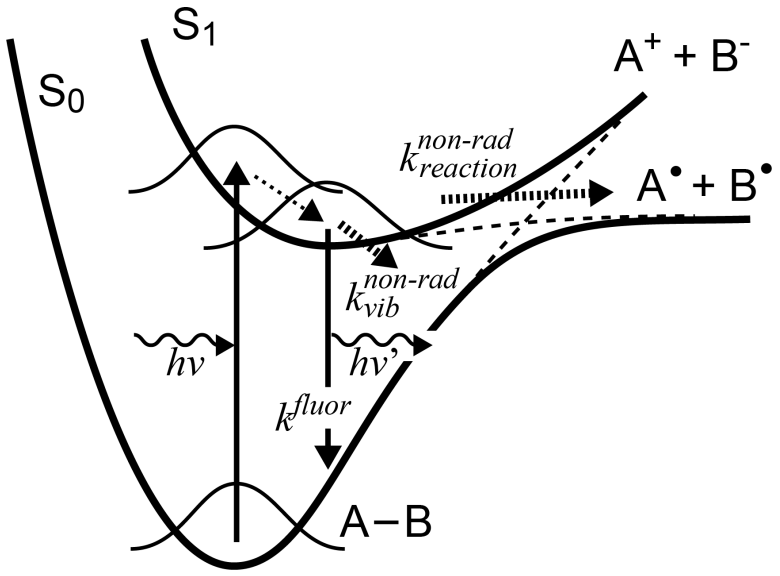

Figure 11.5 Competition of excited state decay paths in a photodissociation reaction of a diatomic molecule, e.g., NaI. The excited state decay paths seen in this simple photoreaction is representative for the more complex photoreaction of retinal in Rh. Thick solid and thin dashed lines represent adiabatic and diabatic potential energy curves, defined in Sect. 11.4. Upon photoabsorption to the FC region (solid upward arrow), a wave packet describing the equilibrated nuclear motion on the ground state potential energy curve, labelled S_0, is lifted to the excited state potential energy curve, labelled S_1, and relaxes then to a nearby potential energy minimum (thin dotted arrow). Subsequently, the excited state population decays via three paths: fluorescence (solid downward arrow), non-radiative decay (thick dashed arrows) to vibrationally excited states of the ground state curve, and non-radiative decay to a photoproduct through an avoided energy curve crossing (discussed in Sect 11.4).

the ground state without emitting a photon, i.e., in a non-radiative way. The non-radiative transitions lead to highly excited nuclear motion in the electronic ground state, the wave function of which matches best that of the pre-transition nuclear motion in the electronic excited state. The non-radiative transitions are described in detail in Sect. 11.5.

Non-radiative transitions that take place between electronic (excited and ground) states of the same spin symmetry are called *internal conversion.* In this case the transition is due mainly to the so-called *non-adiabatic coupling* originating from the nuclear kinetic energy operator $\hat{T}_N(\mathbf{R})$. The system wave function in the BO-approximation is factored into an electronic wave function $\Psi(\mathbf{r}, \mathbf{R})$, the solution of Eq. (11.3), and a nuclear wave function

$\Phi(\mathbf{R})$. Considering presently only the electronic wave function, $\Psi_I(\mathbf{r},\mathbf{R})$, that defines through Eq. (11.3) the electronic state potential energy surfaces E_I^{BO}, the non-adiabatic coupling that is added to the wave equation for the nuclear motion $\Phi(\mathbf{R})$ is

$$\langle \Psi_J(\mathbf{r},\mathbf{R})|\hat{T}_N(\mathbf{R})|\Psi_I(\mathbf{r},\mathbf{R})\rangle_r \simeq -i\hbar \sum_A^{N_{nuc}} d_{JI}^A(\mathbf{R})\ \frac{\hbar}{iM_A}\nabla_A\ , \tag{11.4}$$

namely, a linear combination of operators acting on $\Phi(\mathbf{R})$. Here M_A is the mass of atom A. The $\mathbf{R}$-dependent coefficients of this operator

$$d_{JI}^A(\mathbf{R}) = \langle \Psi_J(\mathbf{r},\mathbf{R})|\nabla_A|\Psi_I(\mathbf{r},\mathbf{R})\rangle_r\ , \tag{11.5}$$

are called the non-adiabatic coupling vectors (Groenhof et al., 2009). In Eq. (11.4), the second derivatives of the electronic wavefunction with respect to the nuclear coordinates, $\mathbf{R}$, are neglected. The role of the operator in Eq. (11.4) is considered further in Sect. 11.5. In Eq. (11.5) $\langle \cdots \rangle_r$ denotes integration over the electronic coordinates.

The non-radiative processes can be discerned indirectly by measuring the *quantum yield of fluorescence*, ϕ^{fluor}, which is defined as the ratio of the number of photons emitted to the number of photons absorbed. If non-radiative transitions do not take place, the number of photons emitted from the population of the excited state would be equal to the number of photons absorbed which produce the population; a measured decrease of the fluorescence quantum yield below unity is indicative of significant non-radiative decay. In this case the actual value of the quantum yield permits one to estimate the speed of the non-radiative decay. For the sake of simplicity, let us assume that the decay process and fluorescence can be described by first order kinetics with rate constants $k^{non-rad}$ and k^{fluor}, respectively. The quantum yield is then

$$\phi^{fluor} = \frac{k^{fluor}}{k^{fluor} + k^{non-rad}}\quad . \tag{11.6}$$

One can conclude that an increased $k^{non-rad}$ leads to a decrease of the fluorescence quantum yield.

11.4 Regulation of Photochemical Processes for Biological Function

Photoinduced processes in proteins are regulated according to the protein's function. Functions are classified as photoactivation as in rhodopsins, lumi-

nescence as in green fluorescent proteins, and light harvesting as in some photosynthetic protein complexes.

For photoactive proteins strong photoabsorption is a prerequisite to attain high sensitivity to incoming light. As photoabsorption cross sections are proportional to the square of the transition dipole moment of the chromophore (Atkins and de Paula, 2009), an optically allowed electronically excited state that contributes a large transition dipole moment is needed. In this regard, the protonated Schiff base of retinal is ideally suited for visual photopigments. The respective characteristics of the optically allowed excited state of retinal is discussed in Sec. 11.6. In addition to the photoabsorption cross section, absorption energy, i.e., the spectral maximum of absorption, is a key factor for visual photopigments. The mechanisms underlying tuning of absorption maxima are discussed in Sec. 11.7.

Control of excited state decay after photoabsorption is also crucial for photorelated protein function. For example, photoactivation requires very different decay channels than does bio-luminescence. In the case of luminescence, the quantum yield of fluorescence, ϕ^{fluor}, is maximized; this also applies to chromophores involved in excitation energy transfer in light harvesting systems. Both types of proteins minimize the role of non-radiative decay. In contrast, photoactivation requires the minimization of fluorescence and the channeling of non-radiative decay towards formation of ground state photoproducts distinct from the initial, i.e., dark, state.

In the case of photoactivative proteins, a large $k^{non-rad}$ is essential for keeping ϕ^{fluor} small as can be concluded from Eq. (11.6). As we noted above, the transition dipole moment of the chromophore in photoactive proteins must be large in order to assure strong absorption of incoming light. Hence, fluorescence from the optically allowed excited state is also fast as the fluorescence rate is also proportional to the square of the transition dipole moment. In order to realize a large quantum yield for photoproduct formation, the respective non-radiative decay channel needs to be much faster in the protein than the fluorescence channel with a typical decay time, i.e., $1/k^{fluor}$, of 1 ns.

Unorganized motion on the excited state surface does not result into motion leading to a specific potential energy crossing point and to subsequent product formation in the ground state. Accordingly, photoactive proteins need to trigger very fast specific motion on the excited state potential energy surface leading to the suitable potential energy crossing point. Typically, the protein environment plays the role of funneling the nuclear motion in the excited state along the desired photochemical reaction coordinate. As mentioned above and discussed in detail below, photochemical reactions of

retinal in rhodopsins are extremely fast and well steered, leading to very weak fluorescence and high quantum yields of photoproduct formation.

11.5 Potential Energy Crossing and Conical Intersection

Photochemical reactions constitute one of the non-radiative processes in chromophores. Figure 11.5 depicts a prototype photochemical reaction process, photodissociation of a diatomic molecule. This process is a one-dimensional analogue of the type of processes occurring in more complex molecules like retinal. In the case of the diatomic molecule, the ground state possesses a potential energy curve along the atom-atom distance with a minimum that corresponds to a stable ionic bond; as the distance increases the potential energy increases steeply and undergoes a so-called *"avoided" energy crossing* (AEC) with a potential energy curve of the covalent excited state of the molecule. Separating the atoms beyond the avoided crossing in Fig. 11.5 leads to dissociation into free neutral atoms.

In the one-dimensional reaction case depicted here, BO energy curves of two states with the same spatial and spin symmetry do not cross (von Neumann and Wigner, 1929). The non-adiabatic coupling term (11.5) contributes to the level repulsion, in particular, in the AEC region where the close energies of two BO states, I and J, give rise to strong non-adiabatic coupling as one can see (note the energy difference in the denominator) from the readily derived expression for the non-adiabatic coupling vector

$$\langle \Psi_J(\mathbf{r},\mathbf{R})|\nabla_A|\Psi_I(\mathbf{r},\mathbf{R})\rangle_r = \frac{\langle \Psi_J(\mathbf{r},\mathbf{R})|[\nabla_A\,,\ \hat{H}_{BO}(\mathbf{r},\mathbf{R})]|\Psi_I(\mathbf{r},\mathbf{R})\rangle_r}{E_I^{BO}(\mathbf{R}) - E_J^{BO}(\mathbf{R})} \quad . \tag{11.7}$$

The commutator $[\nabla_A\,,\ \hat{H}_{BO}(\mathbf{r},\mathbf{R})]$ in this expression corresponds to multiplying the wave function $\Psi_I(\mathbf{r},\mathbf{R})$ by the function $[\nabla_A \hat{H}_{BO}(\mathbf{r},\mathbf{R})]$, the square brackets $[\cdots]$ denoting that ∇_A only acts on $\hat{H}_{BO}(\mathbf{r},\mathbf{R})$, but not beyond the brackets. $[\nabla_A \hat{H}_{BO}(\mathbf{r},\mathbf{R})]$ represents the electrostatic force acting on atom A; since this force is a smooth, but non-constant, function of $\mathbf{R}$ in the AEC region, the coupling expressed through Eq. (11.7) becomes very strong at the AEC due to the energy difference denominator in (11.7) and noticing l'Hospital's rule.

The rate of non-radiative decay which competes against fluorescence, therefore, can proceed quickly along a non-adiabatic transition at an AEC. In general, the non-radiative decay rate, $k^{non-rad}$, involving two parallel channels described by rate constants $k_{vib}^{non-rad}$ (rate of transition from the vibrationally relaxed states from which fluorescence also occurs) and $k_{reaction}^{non-rad}$

(rate of transition through AEC for the photochemical reaction channel, see Fig. 11.5) is approximately

$$k^{non-rad} = k_{vib}^{non-rad} + k_{reaction}^{non-rad} \quad . \tag{11.8}$$

In polyatomic molecules, non-radiative decay through energy curve crossing requires consideration of more than one coordinate for the nuclear motion. Experimentally, many organic molecules have been found to exhibit remarkably small quantum yields of fluorescence, suggesting effective pathways for non-radiative decay through energy crossing. The observed non-radiative decays proceed on a time scale of picoseconds or shorter, which is comparable with the time scale of intramolecular vibrational relaxation after photoexcitation to the FC region. This fast non-radiative decay can be explained through non-adiabatic transition at so-called *conical intersections* (CIs) (Groenhof et al., 2009). Figure 11.6a depicts schematically two BO potential energy surfaces around a CI. The two BO potential energy surfaces touch each other at the CI point, described here in a two dimensional coordinate space, a linear subspace of the configuration space of $3N_{nuc} - 6$ degrees of freedom. The small energy gap of the BO energy surfaces near the CI point drastically accellerates the non-adiabatic transition just as it does in the one-dimensional case shown in Fig. 11.5.

The CI with the peculiar potential energy profile shown in Fig. 11.6a is easily demonstrated as follows. For the sake of simplicity let us consider a CI between the first excited state and the ground state. First, the two adiabatic electronic wavefunctions, $\Psi_1(\mathbf{r}, \mathbf{R})$ and $\Psi_0(\mathbf{r}, \mathbf{R})$, defined by Eq. (11.3), are transformed through a unitary transformation, $\hat{U}(\mathbf{R})$, to *diabatic* ones where the non-adiabatic coupling, given by Eq. (11.4), is minimized to a near zero value

$$\tilde{\Psi}_{1,0}(\mathbf{r}, \mathbf{R}) = \hat{U}(\mathbf{R})\Psi_{1,0}(\mathbf{r}, \mathbf{R}) \quad , \tag{11.9}$$

$$\langle \tilde{\Psi}_1(\mathbf{r}, \mathbf{R}) | \hat{T}_N(\mathbf{R}) | \tilde{\Psi}_0(\mathbf{r}, \mathbf{R}) \rangle_r \simeq 0 \quad . \tag{11.10}$$

Here $\tilde{\Psi}_1(\mathbf{r}, \mathbf{R})$ and $\tilde{\Psi}_0(\mathbf{r}, \mathbf{R})$ represent the diabatic electronic wavefunction of the excited state and the ground state, respectively. For a one dimensional reaction of a diatomic molecule, diabatic wavefunctions that exactly eliminate the non-adiabatic coupling can be determined readily. However, it is not possible to find such a unitary transformation between two states eliminating the non-adiabatic coupling for polyatomic molecules since all coordinate components of the non-adiabatic coupling vector, Eq. (11.5), need to vanish in this case. However, one can choose a reaction coordinate along

which the non-adiabatic coupling is minimized, determining in this way the unitary transformation.

The Hamiltonian matrix $\hat{H}_{BO}(\mathbf{r}, \mathbf{R})$ in the basis of the diabatic electronic wavefunctions is no longer diagonal. We express this matrix

$$\hat{H}_{BO}(\mathbf{r}, \mathbf{R}) = \begin{pmatrix} \tilde{W}_1(\mathbf{R}) & \tilde{V}(\mathbf{R}) \\ \tilde{V}(\mathbf{R}) & \tilde{W}_0(\mathbf{R}) \end{pmatrix} \quad , \tag{11.11}$$

where the diagonal elements, $\tilde{W}_{1,0}(\mathbf{R})$, can be regarded as potential energies of the so-called diabatic states. Unlike adiabatic potential energies, the diabatic ones can cross. In a one-dimensional reaction of a diatomic molecule, the off-diagonal element $\tilde{V}(\mathbf{R_c})$ at the crossing point, $\mathbf{R_c}$, in general, is non-zero unless the spatial and spin symmetries of the two electronic states don't match. Thus the crossing of the energy curves of the adiabatic states with the same spatial and spin symmetries is "avoided", with a minimal energy gap of $2\tilde{V}(\mathbf{R_c})$.

In the case of diabatic potential energy surfaces existing in a configurational space of dimension higher than two, one can find a point, $\mathbf{R_{Cl}}$, where the potential energies cross, i.e., where $\tilde{W}_1(\mathbf{R_{Cl}}) - \tilde{W}_0(\mathbf{R_{Cl}}) = 0$ and $\tilde{V}(\mathbf{R_Cl}) = 0$ hold simultaneously. Since diagonal elements are degenerate and off-diagonal elements vanish at the crossing point, energies in the adiabatic representation obtained by the inverse unitary transformation are also degenerate, i.e., it holds $E_1^{BO}(\mathbf{R_{Cl}}) - E_0^{BO}(\mathbf{R_{Cl}}) = 0$. Taylor expansion of the adiabatic potential energy surfaces around $\mathbf{R_{Cl}}$, the CI point, determines two directions $\mathbf{g}$ and $\mathbf{h}$ in the configuration space along which the adiabatic potential energies separate:

$$\mathbf{g} \equiv \nabla_{\mathbf{R}}[E_1^{BO}(\mathbf{R}) - E_0^{BO}(\mathbf{R})]|_{\mathbf{R}=\mathbf{R_{Cl}}} \quad , \tag{11.12}$$

$$\mathbf{h} \equiv \nabla_{\mathbf{R}}\langle\Psi_1(\mathbf{r}, \mathbf{R})|\hat{H}_{BO}(\mathbf{r}, \mathbf{R})|\Psi_0(\mathbf{r}, \mathbf{R})\rangle_r|_{\mathbf{R}=\mathbf{R_{Cl}}} \quad . \tag{11.13}$$

Here $\nabla_{\mathbf{R}}$ indicates the gradient operator with respect to all nuclear coordinates. $\mathbf{g}$ and $\mathbf{h}$ are called *gradient difference vector* and *derivative coupling vector*, respectively. The cone shape of the potential energy profile, therefore, is represented in a two-dimensional space spanned by $\mathbf{g}$ and $\mathbf{h}$. It is noteworthy that the zero-dimensional CI point in the two dimensional space of $\mathbf{g}$ and $\mathbf{h}$ constitutes a CI seam in the remainder of the $(3N_{nuc}-8)$-dimensionsional configurational space, a ubiquitous feature of the conical intersection for polyatomic molecules.

The transition rate of non-radiative decay through the CI region is not properly accounted for by a perturbative approach such as Fermi's golden

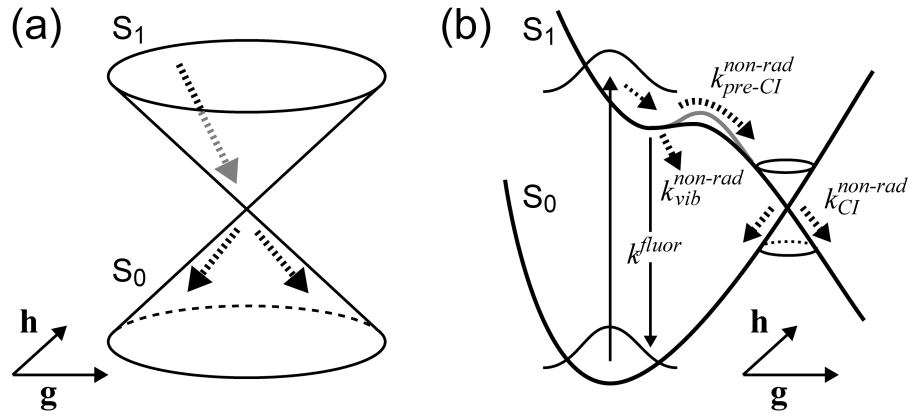

Figure 11.6 (a) Schematic representation of a conical intersection. A trajectory proceeding on the excited state BO potential energy surface (upper cone) undergoes an electronic transition near the conical intersection (CI) point at which apexes of two cones of the excited state and ground state touch in a coordinate space spanned by vectors **g** and **h** defined in Eqs. (11.12, 11.13). After the transition, the trajectory moves quickly on the ground state BO potential energy surface (lower cone) down the energy gradient. (b) Competition of excited state decay paths. Since the rate of non-radiative transition at the CI is fast, the rate of the overall non-radiative transition is determined mainly by the rate at which trajectories reach the CI region.

rule because of a typically large non-adiabatic coupling and the close proximity of two energy levels. Furthermore, in such strong coupling case, the transition rate depends explicitly on the nuclear motion on the BO potential energy surfaces. In principle, nuclear wave packet motion representing the molecular dynamics and the electronic transition need to be described by the time-dependent Schrödinger equation for the nuclear motion with multi-electronic state coupling of the non-adiabatic interaction given by Eq. (11.4). However, for polyatomic molecules the needed calculations become quickly too formidable of a task, but a semi-classical treatment is feasible. In such treatment, the nuclear motion on a single potential energy surface is described classically. In the adabatic representation, a trajectory of the nuclear motion on the I-th BO potential energy surface is calculated by numerically solving Newton's equation

$$M_A \ddot{\mathbf{R}}^I_A(t) = -\frac{\partial E^{BO}_I(\mathbf{R})}{\partial(\mathbf{R}_A)} \quad , \tag{11.14}$$

where $\mathbf{R}^I_A(t)$ expresses a trajectory of the A-th atom on the I-th BO surface. Then, along the classical trajectory, the transition between two electronic

states is represented by a transition between two BO surfaces induced by the non-adiabatic coupling. The relevant coupling element between two BO electronic states in a semi-classical representation is

$$\langle \Psi_J(\mathbf{r},\mathbf{R})|\hat{T}_N(\mathbf{R})|\Psi_I(\mathbf{r},\mathbf{R})\rangle_r \simeq -i\hbar \mathbf{d}_{JI}(\mathbf{R})\cdot\dot{\mathbf{R}}(t) \quad , \tag{11.15}$$

where the quantum mechanical momentum operator in Eq. (11.4) has been replaced by the corresponding classical velocity. The non-adiabatic coupling is then expressed through the scalar product of the non-adiabatic vector already introduced, $\mathbf{d}_{JI}(\mathbf{R})$, and the velocity of nuclear motion.

For a one-dimensional reaction, the transition probability for an AEC can be evaluated by Landau-Zener (LZ) theory, which provides a simple formula for the transition probability (Zener, 1932). In this theory, three assumptions are introduced: (i) the velocity, $\dot{R}(t)$, is constant, (ii) the energy difference between the two diabatic states, $\Delta\tilde{W}(R(t)) = \tilde{W}_1(R(t)) - \tilde{W}_0(R(t))$, varies linearly with time along the trajectory, and (iii) the off-diagonal coupling element between the two diabatic states is constant, i.e., $\tilde{V}(R(t)) = \tilde{V}$. With these assumptions, the transition probability between two adiabatic states, P_{LZ}^{ad}, is (Desouter-Lecomte and Lorquet, 1979)

$$P_{LZ}^{ad} = \exp\left[-\frac{\pi}{4\hbar}\left|\frac{\Delta E^{BO}(R_c)}{\dot{R}d_{10}(R_c)}\right|\right] \quad , \tag{11.16}$$

where $\Delta E^{BO}(R_c) = E_1^{BO}(R_c) - E_0^{BO}(R_c) = 2\tilde{V}$, is the energy difference between the two adiabatic states at the crossing point, R_c. As seen in Eq. (11.16), the probability of the transition between two adiabatic states becomes large when $\Delta E_{BO}(R_c)$ is small, the velocity is large, and the non-adiabatic coupling element, $d_{10}(R_c)$, is large.

For the transition between multi-dimensional potential energy surfaces of a polyatomic molecule, the one-dimensional description by LZ theory may lead to a difficulty in evaluating the transition probability due to the complex character of the potential energy surfaces and the non-adiabatic coupling. In particular, in the CI region, the off-diagonal coupling element between diabatic states, $\tilde{V}(\mathbf{R})$, can depend strongly on the nuclear coordinates, which violates the assumption underlying LZ theory. Nevertheless, the simple formulation of LZ theory provides valuable insight into the electronic transition of an AEC, even for complex systems.

The multi-electronic state dynamics of polyatomic molecules is often treated by Tully's fewest-switches surface hopping algorithm (Tully, 1990). According to this algorithm, the probability for hopping between surfaces is determined by numerically solving a time-dependent Schrödinger equation for

the population of the adiabatic electronic states. In the case of a process including two electronic states, the respective Schrödinger equation is

$$i\hbar \begin{pmatrix} \dot{c}_1(t) \\ \dot{c}_0(t) \end{pmatrix} = \begin{pmatrix} E^1_{BO}(\mathbf{R}(t)) & -i\hbar \mathbf{d}_{10} \cdot \dot{\mathbf{R}}(t) \\ -i\hbar \mathbf{d}_{01} \cdot \dot{\mathbf{R}}(t) & E^0_{BO}(\mathbf{R}(t)) \end{pmatrix} \begin{pmatrix} c_1(t) \\ c_0(t) \end{pmatrix} \quad , \quad (11.17)$$

where $c_{1,0}(t)$ represents expansion coefficients of the two adiabatic electronic states. The off-diagonal elements for the coupling between the adiabatic states is the semi-classical non-adiabatic coupling given by Eq. (11.15).

The Schrödinger equation is solved along a classical trajectory $\mathbf{R}(t)$ on the potential energy surface of the representative state, the population of which is supposed to be dominant. For example, initially the 1-st adiabatic state may be populated. The probability of hopping to the 0-th state, P^{ad}_{Tully}, in a time step of the integration of the Schrödinger equation is

$$P^{ad}_{Tully} = \max\left[0, \frac{-\dot{\rho}_{11}\Delta t}{\rho_{11}}\right] \quad , \quad (11.18)$$

where Δt is the time step and $\rho_{11} = |c_1(t)|^2$ is the population of the 1st adiabatic state. The decision for a hop is made by comparing the transition probability (11.18) with a random number. After the transition occurs, the trajectory is calculated on the 0-th state and the population change is also evaluated by the Schrödinger equation with the trajectory. Statistical sampling of the trajectory provides one with ensemble averages of the population decay. Extension to multi-electronic transitions more than two is straightforward.

A more general and detailed description is found in (Groenhof et al., 2009; Tully, 1990). It is known that Tully's surface hopping approach has defects for re-transition from the lower to the upper state due to inconsistency of the mixed quantum-classical treatment. However, re-transition by AEC in the CI region for a polyatomic molecule is rare since the conical shape of the potential energy surface of the lower state facilitates intramolecular vibrational relaxation that prevents the trajectory from re-entering the CI region.

The CI serves as the predominant channel for non-radiative decay. The excited state population that falls into the potential energy funnel of the CI region cannot escape from the region, like an ant entrapped in a doodlebug's pit; instead, it quickly undergoes non-adiabatic transition to the ground state. The remarkable efficiency for the non-adiabatic transition through a CI together with its ubiquitous feature has brought about a paradigm shift for the mechanisms underlying non-radiative decay in polyatomic molecules. It is now recognized that the rate of a very fast non-radiative decay is deter-

mined not by how fast the non-adiabatic transition proceeds at the energy crossing region, but by how fast the excited state population reaches the CI region, as schematically depicted in Fig. 11.6b.

We like to demonstrate the stated behavior through a simple kinetic description. Let us define by $k_{pre-CI}^{non-rad}$ and $k_{CI}^{non-rad}$ the rate of reaching the CI region in the first place and the rate of transition at the CI region, respectively. Since the two events take place sequentially, the overall rate of non-radiative decay for the photochemical reaction through CI, $k_{pre-CI}^{non-rad}$, is given by the approximate expression

$$\frac{1}{k_{reaction}^{non-rad}} \approx \frac{1}{k_{pre-CI}^{non-rad}} + \frac{1}{k_{CI}^{non-rad}} \quad . \tag{11.19}$$

Obviously, for $k_{CI}^{non-rad} \gg k_{pre-CI}^{non-rad}$ holds $k_{reaction}^{non-rad} \simeq k_{pre-CI}^{non-rad}$. Thus, according to Eqs. (11.8, 11.19), the process competing against fluorescence is the motion towards a CI region and not the transition at a CI.

The excited state process before reaching the CI region, therefore, is the primary target for control through the protein environment for a photoactive protein to realize its function effectively. In the case of rhodopsins, as seen below, the molecular dynamics before reaching the CI region is crucial for the sensory efficiency of the receptor. Crucial is also the branching ratio among possible chemically different photoproducts. Molecular dynamics simulations describing the approach to CI regions and branching ratios after crossing to the ground state are extremely helpful for revealing the role of the protein environment into steering the two processes (approach to CIs and branching) and, presently, the only means to obtain closer insight. Such simulations of excited state conformational dynamics are extremely challenging, but possible (Hayashi et al., 2003, 2009).

11.6 Electronic Structure of Protonated Schiff Base Retinal

The common chromophore of retinal proteins is retinal bound as a PSB to lysine. Retinal consists of a linear polyene chain with six conjugated double bonds. The long π-conjugation of the polyene chain together with a positive charge of the Schiff base group located at one end of the polyene gives rise to strong optical absorption in the visible region of the spectrum. The absorption is due to a so-called π-π^* excitation.

The electronic structure of linear polyenes has been the subject of photophysical studies since many decades. The optically allowed π-π^* absorption band of a linear polyene with six conjugated double bonds arises in an ultraviolet region (320$\sim$370 nm). The corresponding excited state possesses ^1B_u

symmetry and is mainly characterized as a single electron excitation from the highest occupied molecular orbital (HOMO) to the lowest unoccupied one (LUMO). In the vicinity of the ^1B_u state, an optically forbidden π-π^* state of ^1A_g symmetry exists along with several other forbidden states. The electronic structure of the ^1A_g excited state is described by multi-configurational excitations that involve two triplet excitations coupled to an overall singlet spin state (Schulten and Karplus, 1972). The ^1A_g state and its sister triplet-triplet states have been investigated computationally in (Ritz et al., 2000; Tavan and Schulten, 1986, 1987); an experimental-theoretical review can be found in (Hudson et al., 1982).

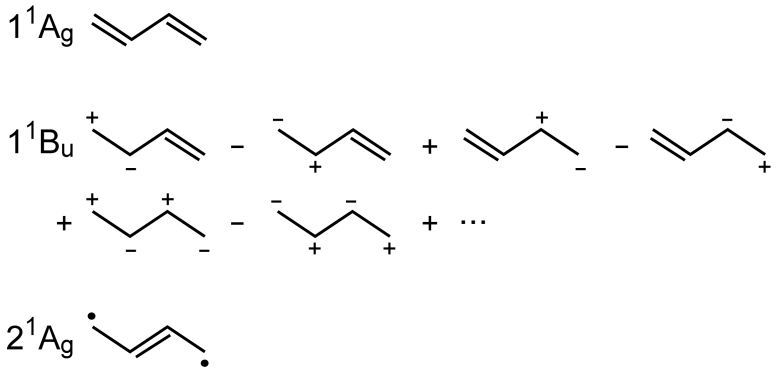

Figure 11.7 Valence bond structures of butadiene in the 1^1A_g ground state, in the 1^1B_u excited sate and in the 2^1A_g excited state. Butadiene is the simplest polyene, involving only two double bonds, i.e., four π-electrons. The 1^1A_g ground state is represented by the familiar, two double bond, covalent valence bond (VB) structure. The optically allowed 1^1B_u state of butadiene is represented by a linear combination of ionic VB structures; the optically forbidden 2^1A_g state of this polyene is mainly represented by a VB structure where two radicals at the two ends of the polyene exhibit a singlet coupling.

The polyene excited states can also be interpreted through a valence-bond (VB) representation (Schulten and Karplus, 1972). Figure 11.7 schematically depicts the main VB electronic cofigurations of the ^1B_u and ^1A_g electronic states. The ^1B_u state is expressed by a linear combination of polar structures. In each of the polar structures, π-electrons are shifted between the carbons constituting a double bond and, thus, polarize the double bond. The ^1B_u state is often called *ionic* because of the polar nature of the VB configurations, although the polarization does not explicitly appear in the one electron density of the total wavefunction due to cancelation by the linear combination. The ionic character is responsible for the large transition

dipole moment that endows the ^1B_u state with strong photoabsorbance. The polarization of π-electrons in each VB configuration induces a counter-polarization of a σ-bond that compensates the π-polarization. Because of this σ,π-polarization, one needs to take into account explicitly dynamic electron correlation between the σ- and π-orbitals for an accurate computation of the electronic energy of the ^1B_u state. In the case of the ^1A_g excited state as well as the ground state, which also possesses ^1A_g symmetry, electronic structures are expressed as a linear combination of covalent Kekule-like and Dewar-like VB structures, as shown in Fig. 11.7, indicating a covalent character for both states.

The electronic excitations of the PSB retinal chromophore in Rh can be delineated from polyene electronic excitations described above. However, the positive charge introduced in the conjugated π electron system through the protonation of the Schiff base linkage to lysine alters remarkably the electronic structure (Schulten et al., 1980). In particular, the absorption spectrum of the optically allowed π-π^* excitation of PSB retinal is considerably red-shifted from that of a polyene with the same number of the conjugated double bonds, coming to lie in the visible region, which is appropriate for the biological function. The positive charge on the PSB induces localization of π orbitals as shown in Fig. 11.8a. One can discern in the figure that retinal's HOMO and LUMO exhibit larger distributions in the β-ionone ring half and in the PSB half, respectively. A HOMO-LUMO single excitation which characterizes mainly the optically allowed ^1B_u-like state involves, therefore, a positive charge transfer from the PSB half to the β-ionone ring half along the polyene chain as shown in Fig. 11.8b. The localization of HOMO and LUMO also contributes to the red-shift of the optically allowed absorption band compared to that of the same length polyene because of reduction of electron correlation. Finally, the positive charge breaks the polyene D_{2h} symmetry in PSB retinal; accordingly, the electronic characters of the ^1B_u-like and ^1A_g-like excited states become mixed, endowing also the ^1A_g-like excited state of retinal with non-zero optical absorbance, albeit only a weak one.

11.7 Mechanism of Spectral Tuning in Rhodopsins

Control of photoabsorption, namely of the wavelength position of the absorption maximum, $\lambda_{\max}$, is functionally important for retinal proteins as discussed above. This control is referred to as spectral tuning. Since all retinal proteins possess a PSB retinal chromophore, i.e., their chromophores are identical (though in some animal species retinal is replaced, to reach longer

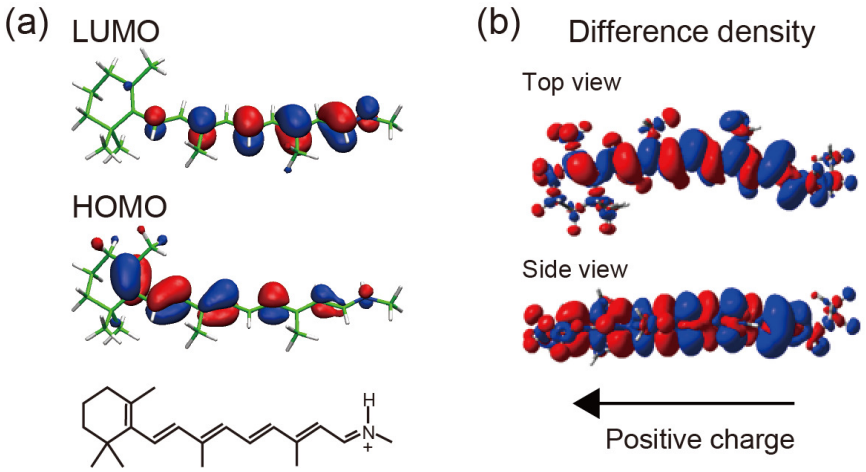

Figure 11.8 (a) Highest occupied moleular orbital (HOMO) and lowest unoccupied molecular orbital (LUMO) of PSB retinal. Depicted is the chemical structure of PSB retinal and superimposed on it the molecular orbitals colored blue and red according to the sign of the orbital wave functions; the characteristic blue-light lobes stem in (a) from the π-electron atomic orbitals. (b) Difference in electron density between the excited state and the ground state (Fujimoto et al., 2010). Red and blue lobes represent in (b) a decrease and increase of the electron density, respectively. Blue and red lobes are bigger on the PSB side (right) and the β-ionone ring side (left), respectively, indicating an overall shift of positive charge along the polyene chain from the PSB side to the β-ionone ring side.

wavelength absorption, by retinal$_2$ with π-conjugation extended in the β-ionone ring by one double bond, a case not considered here), interaction of the chromophore with the protein environment is responsible for the needed variation of absorption maxima. As the excitation energy is defined as the energy difference between the B_u-like excited state and the ground state, spectral tuning is based on the different effect of the protein environment on the energies of the two states. Indeed, the molecular mechanism of color tuning in rhodopsins exploits differences in the electronic character between the states that has been described in Sect. 11.6. The spectral shift originates mainly from conformational change of the chromophore and from electrostatic interaction between chromophore and polar groups in the surrounding protein.

Conformational changes of the PSB retinal chromophore are induced by confinement due to steric interactions in the binding pocket, in which the chromophore is situated, and due to hydrogen-bonding of retinal's PSB to polar amino acid side groups. The polyene chain of PSB retinal can be de-

formed torsionally in the ground state; however, π- π^* excitation alters significantly the torsional flexibility of retinal. One can recognize in Fig. 11.8a that the HOMO exhibits bonding and anti-bonding phases at double and single bonds in the polyene chain, respectively, and that the phase behavior of the LUMO is opposite to that of the HOMO, bonding and anti-bonding phases for the LUMO appearing at single and double bonds, respectively. Hence, torsions around double and single bonds cause decrease and increase of the HOMO-LUMO energy gap, respectively, leading to respective red and blue shifts of the absorption maxima of the π- π^* excitations.

We illustrate the role of torsion on the HOMO-LUMO energy gap and, thereby, on the $\lambda_{\max}$ of retinal for the C_6-C_7 bond (for the numbering of carbon atoms see Fig. 11.2). Torsion around this bond has little effect on the HOMO energy as the orbital exhibits an anti-bonding phase for this bond; however, the same torsion increases the LUMO energy as the latter orbital exhibits a bonding phase for the C_6-C_7 bond. In spite of the preference for planarity as part of retinal's π-conjugated bond system, the C_6-C_7 bond in retinal rotates rather readily due to steric interactions of the H_7 atom with methyl groups at positions C_1 and C_6. Quantum chemistry calculations demonstrate a steep increase in excitation energy with torsion around the C_6-C_7 bond (Wanko et al., 2005). Thus, torsion around the C_6-C_7 bond can control retinal's absorption maximum in rhodopsins; in fact, the C_6-C_7 torsional angles of the chromophore in bR and Rh differ remarkably (deviation from planarity is $\sim 10^\circ$ and $\sim 50^\circ$ in bR and Rh, respectively) and explain the blue shift from the bR to the Rh spectral maximum (Fujimoto et al., 2007).

Electrostatic interaction between retinal chromophore and protein polar and charged amino acids also plays a central role in spectral tuning. As described above (see also Fig. 11.8b), PSB retinal excitation involves a charge shift along the polyene backbone. Hence, an electrostatic field along the polyene chain due to surrounding polar groups can shift the PSB retinal spectrum. Since upon photoexcitation the positive charge of the Schiff base moves toward the β-ionone ring, the excitation energy increases if in a retinal protein the electrostatic potential becomes more negative near the Schiff base and more positive near the β-ionone ring.

In retinal proteins, carboxylate groups such as Asp85 and Asp212 for bR and Glu113 for Rh serve as counter anions of the PSB and provide large contributions to the spectral shifts. In chloride pump proteins, i.e., halorhodopsin (Scharf and Engelhard, 1994) and a D85T mutant of bR (Sasaki et al., 1995), a chloride anion bound in the vicinity of the PSB also affects the absorption maximum strongly; removal of the bound chloride

anion results in a spectral red-shift. In addition to the counter ion groups, polar groups surrounding the chromophore such as hydroxyl groups of serine and threonine as well as water molecules can contribute to spectral shifts. Among bacterial retinal proteins, bR and sRII exhibit a remarkable difference between their absorption spectra, i.e., $\lambda_{\max} = \sim 570$ nm for bR and $\lambda_{\max} = \sim 500$ nm for sRII, whereas X-ray crystallographic studies revealed only a slight difference in the chromophore structure. Comprehensive mutagenesis studies for sRII (Shimono et al., 2000) and theoretical investigations (Hayashi et al., 2001; Hoffmann et al., 2006; Ren et al., 2001) have shown that a major part of the spectral shift can be attributed, in case of these pigments, to a difference in electrostatic interaction with the surrounding polar and charged amino acids.

As mentioned above, the retina of the human eye contains three color receptors, namely, human red (HR), human green (HG), and human blue (HB) receptors. An explanation of the receptors' spectral tuning is of great interest. Unfortunately, biochemical and structural information on the color receptors is sparse, in particular, no iodopsin structure has been determined yet. However, biochemical and mutagenesis studies revealed that polar protein groups and a chloride ion at a binding site on the extracellular side of the protein give large contributions to the spectral shifts (Shichida and Imai, 1998). Computationally, an attempt by means of quantum chemistry calculations (Fujimoto et al., 2009) has been made with model protein structures for the color receptors constructed based on the available Rh structure. The latter study suggests that electrostatic interaction contributes to the spectral shifts between the three receptors; a chromophore structural difference appearing in HB appears to produce the significant blue shift for this receptor.

11.8 Photoisomerization of Retinal in Rhodopsins

Photoabsorption of retinal initiates dynamics on the excited state surface that leads to strong torsional motion in the polyene chain moiety. As described above, the S_1 state responsible for the photoabsorption and the photochemical reaction possesses ionic valence-bond configurations. Since these ionic configurations prefer reduction of overlap between 2p orbitals constituting the π molecular orbitals at a double bond of the polyene, one of the polyene double bonds undergoes torsion towards a 90^o conformation. A remarkable charge separation, the so-called sudden polarization (Bonačić-Koutecky et al., 1984; Salem, 1979) occurs in the twisted conformation, which can make energy levels of excited state and ground state approach

each other to form a CI. In the case of a PSB polyene, the ground state positive charge is localized in the Schiff base half of retinal and the excited state positive charge in the β-ionone ring half, the two halves being separated by the isomerizing bond (González-Luque et al., 2000). Through the conical intersection arising for perpendicular torsion of the bond, the excited state population decays to the ground state where the perpendicular geometry relaxes to the planar one, the relaxation involving branching either back to the original isomeric state of the double bond or to the alternative isomeric state.

The photoisomerization reactions in rhodopsins are known to be the fastest molecular reactions in nature. The time constants for excited state decay in the proteins are measured to lie in the range 50-500 fs. The fast decay diminishes ϕ^{fluor} (Eq. (11.6)), avoiding nearly completely decay through fluorescence, and provides a high photoactivation quantum yield of more than 0.6, the value being determined by the branching ratio of completion or lack of completion of the isomerization reaction after crossing through the CI. In fact, ϕ^{fluor} has been measured experimentally to be only $\sim 10^{-5}$ (Kochendoerfer and Mathies, 1996).

The actual photoisomerization in the various rhodopsins exhibits strict stereoselectivity. For example, in bR, the photoisomerization of the chromophore, which is in the all-trans state in the resting ground state, produces only the 13-cis isomer or returns to the all-trans state, even though other double bonds in the polyene chain, in principle, are capable of undergoing isomerization. The extremely fast reaction rates and the strict stereoselectivity are due to steering by the protein environment. In fact, the photoisomerization reaction time constant of retinal in methanol solvent is 2.5-4 ps (Logunov et al., 1996) and photoisomerization from the all-trans configuration in this solvent is not stereoselective: photoproducts include 9-cis, 11-cis, and 13-cis isomers with quantum yields of 0.02, 0.14, and 0.01, respectively (Koyama et al., 1991). Steering by the protein environment towards the proper photoproducts speed-up the reaction, by a factor 10 to 100, and increases the quantum yield, thus, furnishing photoreceptors with high sensitivity to incoming light.

The stated behavior can be clearly seen in the photoreactions of Rh and bR. The photoisomerization of Rh taking place from 11-cis retinal to all-trans retinal proceeds within the extremely short time of $\sim$50 fs and with a high quantum yield, namely 0.68, without any by-product other than the 11-cis reactant form (Kochendoerfer and Mathies, 1996; Polli et al., 2010). In bR, the photoisomerization from all-trans to 13-cis retinal occurs witin 240-500 fs (Gai et al., 1998), slightly slower than the reaction

in Rh, and with a quantum yield of 0.6. Interestingly, the kinetic behavior differs remarkably between Rh and bR. Pump-probe experiments on Rh (Polli et al., 2010; Wang et al., 1994) revealed coherent (or synchronous in a classical mechanical sense) wave packet dynamics from the FC region to the photoproduct even in the presence of thermal noise in the surrounding protein environment. In contrast, pump-dump-probe experiments on bR (Ruhman et al., 2002) saw photoproduct formation to proceed in an incoherent, stochastic manner (asynchronous in a classical mechanical sense), although synchronous vibrations were observed in the excited state (Kobayashi et al., 2001). Apparently, in the case of Rh excited state motion occurs synchronously along a single path, whereas in bR excited state dynamics is funneled briefly into a multi-dimensional basin of attraction from where the system escapes asynchronously through a relatively narrow exit that leads to photoproduct formation. The difference in kinetic behavior between Rh and bR gives a clue for understanding the physical mechanism underlying photoreaction steering in rhodopsins.

A key role of the protein environment is to achieve an optimal branching ratio by targeting, during the excited state motion, the CI with the 90^o rotation of the right double bond and, after crossing through the CI, by completing the bond rotation to reach the desired isomeric state. Figure 11.9 depicts schematically the potential energy profile of the isomerization reaction. Upon photoabsorption, the reactant isomer in the resting ground state is vertically excited to the FC region in the excited state where the isomer is located at the top of a potential hill with a single peak. From the FC region, downhill paths connecting to different isomers through alternative CIs are possible. One can discern from Figure 11.9 that the branching ratio is determined in two regions, namely, in the FC and CI regions. First, dynamics in the FC region determines stereoselectivity, i.e., the trajectory on the excited state energy surface must be steered by the protein environment towards the CI corresponding to 90^o torsion around the selected bond. Once a trajectory falls into any one of the branching paths, it never comes back out of the CI to reach the CI of an alternative bond as the crossing at a CI is too fast. Second, the protein environment must assure that, after crossing at the right CI, when torsion of the selected double bond is at a 90^o angle, bond rotation has a good chance to complete and form the new isomeric state of retinal; the protein environment and the chromophore properties must prevent that too many CI crossings fall back to the reactant isomeric state.

As mentioned above, experimental evidence suggests that, in the protein environment of Rh and bR, no byproduct isomers other than the product

and reactant ones are generated by the photoreaction. Hence, the dynamics at the FC region is strictly regulated for the selectivity of the isomerizing bond. How is such strict selectivity achieved? Recent molecular simulation studies have suggested a striking contrast between the mechanisms in Rh and bR (Hayashi et al., 2003, 2009).

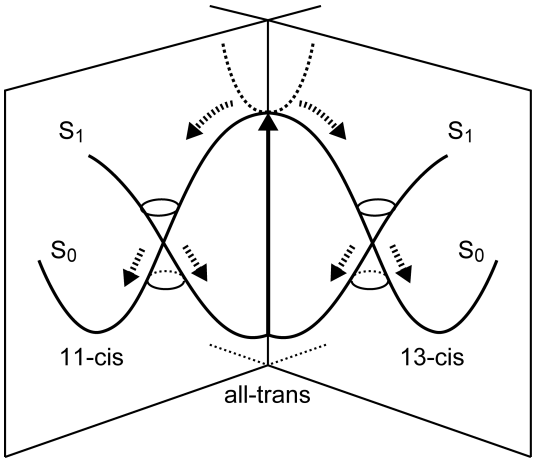

Figure 11.9 Potential energy profiles governing photoisomerization of PSB retinal from an all-trans configuration to two possible product isomeric states, 11-cis and 13-cis. The branching ratio of the product isomers is determined by dynamics in two regions, the FC and the CI region.

In bR, the interaction of the chromophore with the protein surroundings that determines bond selectivity is exerted on the dynamics in the excited state. A simulation of excited state trajectories without protein surrounding showed that thermal fluctuation existing at the moment of vertical transition by photoabsorption leads to formation of several isomers. Obviously, in bR, the paths to "wrong" CIs are blocked by protein-chromophore interaction and all trajectories are funneled to the proper CI connecting to the 13-cis isomer.

In Rh, protein-chromophore interaction does not play a major role in the excited state dynamics. Room temperature simulations showed that thermal fluctuation before vertical transition and protein-chromophore interaction in the excited state do not significantly alter the Rh isomerization trajectories (Hayashi et al., 2009). This indicates that bond-selectivity is due to intrinsic properties of 11-cis retinal in its reactant conformation in the resting ground state. In fact, the dihedral angle around the isomerizing bond, C_{11}=C_{12}, in 11-cis retinal's reactant conformation is found sufficiently twisted, namely by 17°, to steer the trajectory upon excitation instantaneously toward the

product isomer. In addition, concerted co-rotations of C_9=C_{10} and C_6–C_7 also promote the isomerization around C_{11}=C_{12} (Frutos et al., 2007; Hayashi et al., 2009; Polli et al., 2010).

The "blocking-and-funneling" and "hands-off" roles of bR and Rh, respectively, during retinal excited state dynamics explain the observed photochemical kinetics very well. In bR, chromophore-protein interaction blocking wrong isomerization paths perturbs the reaction dynamics, leading to asynchronous motion after vertical excitation and decreasing the escape rate from the FC region. On the other hand, the hands-off mechanism of Rh avoids collision between isomerizing chromophore and protein environment, thus, maximizing the reaction rate.

Once a branching path from the FC region toward a product conformer is selected in Rh or bR, the trajectory along the branching path undergoes in the CI region an electronic transition to the ground state; subsequently, the trajectory undergoes another branching, namely, between reactant and product isomeric states. In either Rh and bR, the branching ratios of product and reactant isomers are larger than 0.6, indicating a preference for the product isomers. This preference can be explained by a simple semi-classical consideration for a one dimensional reaction case (Weiss and Warshel, 1979). Figure 11.10 depicts a schematic mechanism for the branching ratio in an AEC region. First, a trajectory enters into the AEC region from the FC region with a momentum toward the product isomer. Passing the AEC region, part of the population associated with the trajectory undergoes electronic transition to the ground state. Because of the momentum moving in the excited state toward the product isomer, the transition produces a trajectory that also has a momentum toward the product isomer in the ground state. The momentum transfer to the ground state can be explained in the framework of LZ theory, Eq. (11.16). The population not crossing to the ground state leaves the AEC region and then re-enters the AEC region with the opposite momentum. The recrossing event gives rise to a ground state trajectory toward the reactant isomer. Further crossings events take place, with alternating directions of momentum until eventually all of the excited state population is divided into populations of the reactant and product conformers in the ground state.

For the process outlined, the branching ratio, Φ, can be determined with the assumption of a constant transition probability, θ, at each crossing event. Summing up all crossing events yields

$$\Phi = (1-f)\Big[\theta + \theta(1-\theta)^2 + \theta(1-\theta)^4 + \ldots\Big] = (1-f)/(2-\theta) \quad , \quad (11.20)$$

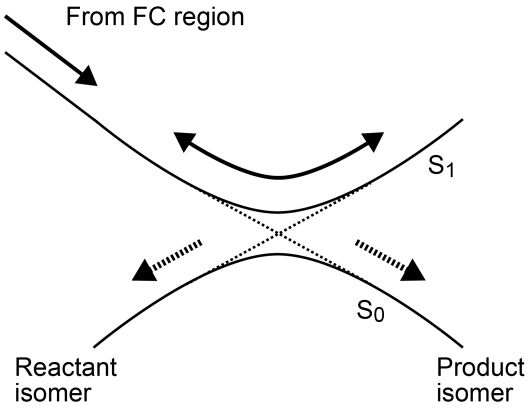

Figure 11.10 Mechanism of population branching at a one-dimensional avoided energy crossing. Solid and dotted lines represent adiabatic and diabatic potential energy curves. A trajectory coming from the FC region in the excited state exhibits oscillation on an adiabatic potential energy curve around the avoided energy crossing (AEC) point. Population associated with the trajectory undergoes transition to the electronic ground state during each passing of the AEC. The momentum at the AEC determines the isomeric state produced in the ground state.

where f represents a population lost before the trajectory enters the AEC region due to fluorescence and non-adiabatic transitions, which is expected to be negligible in the case of Rh and bR because of their fast photoisomerization rates. The equation suggests that the branching ratio approaches one for $\theta \to 1$ and the lower bound of 0.5 for $\theta \to 0$. Branching ratios greater than 0.6, as observed for Rh and bR, are achieved for $\theta > 0.33$. One can discern from Eq. (11.20) that the dominating contribution to the branching ratio stems from the term which corresponds to the first crossing event.

In case of isomerization in the protein environment, the trajectory proceeds on a multi-dimensional potential energy surface. A quantum chemical molecular dynamics study with a surface hopping approach for bR, which took all degrees of freedom involved in the reaction process into account, showed that the recrossing events after the first crossing in the CI region are random rather than exhibiting regular alternate repeats as assumed in Eq. (11.20) due to multi-dimensional intramolecular vibrational coupling (Hayashi et al., 2003). Nevertheless, in the mult- dimensional case the first crossing event was observed to lead exclusively to a ground state trajectory moving toward the product isomer as seen in the model discussed above.

11.9 Summary and Outlook

In this chapter, the mechanisms of spectral tuning and photoisomerization in retinal proteins were discussed in conceptual terms. Through many experimental and theoretical studies carried out over several decades, understanding of the quantum physics and quantum chemistry of the primary photoactivation events in rhodopsins has been significantly advanced. Because of the relative simplicity of the structures of rhodopsins and the rather straightforward reaction dynamics involved in photoactivation, rhodopsins have been one of the most extensively studied systems targeted for elucidation of quantum effects in biological function. There remain, however, important issues that are not yet understood and need to be addressed in future studies. For example, the photoisomerization reactions have been suggested experimentally and theoretically to involve not only the rotational motion around the isomerizing bond, but also other molecular motions such as in-plane relaxation of the bond-alternation of the polyene, hydrogen-out-of-plane motion and C-H bond bending motion, as well as concerted co-rotations in the polyene chain (Frutos et al., 2007; Hayashi et al., 2003; Kobayashi et al., 2001; Kukura et al., 2005). The coupling of these various motions to photoisomerization still needs to be fully investigated. Molecular dynamics simulations at electronic and atomic resolution becoming more and more feasible today promise more insight into the quantum physics of retinal proteins, for example quantum coherent control of photoisomerization as demonstrated recently experimentally in the case of bR (Prokhorenko et al., 2006).

Eighty years ago, Gorge Wald discovered the role of retinal in animal vision (Wald, 1933). Retinal has been extensively studied ever since, attracting in particular theoretical and computational scientists to biology due to the molecule's highy correlated σ, π-electron system. Retinal's remarkable role in vision, achieved through its strong light absorption, wide range of $\lambda_{\max}$ values tuned readily through changes of its protein environment, and capability for highly specific isomerization reactions, is still admired today and still subject of intense investigations.

11.10 Acknowledgment

The authors are grateful to Kazuhiro Fujimoto, Ryoichi Kida, Olga Svinarski and Bo Liu for assistance with drawing of figures. This work was supported by National Science Foundation grant MCB0744057 and National Institutes of Health grant P41-RR05969 (to K. S.).

References

Atkins, P., and de Paula, J. 2009. *Physical Chemistry*. 9th edn. Oxford University Press.

Beja, O., Aravind, L., Koonin, E.V., Suzuki, M.T., Hadd, A., et al. 2000. Bacterial rhodopsin: evidence for a new type of phototrophy in the sea. *Science*, **289**, 1902–1906.

Birge, R.R. 1990. Nature of the primary photochemical event in rhodopsin and bacteriorhodopsin. *Biochimica et Biophysica Acta*, **1016**, 293–323.

Bonačić-Koutecky, V., Kohler, J., and Michl, J. 1984. Prediction of structural and environmental effect on the S1-S0 energy gap and jump probability in double-bond cis-trans photoisomerization. A general rule. *Chemical Physics Letters*, **104**, 440–443.

Desouter-Lecomte, M., and Lorquet, J.C. 1979. Nonadiabatic interactions in unimolecular decay. IV. Transition probability as a function of the Massey parameter. *Journal of Chemical Physics*, **71**, 4391(13 pages).

Frutos, L.M., Andruniów, T., Santoro, F., Ferré, N., and Olivucci, M. 2007. Tracking the excited-state time evoluation of the visual pigment with multiconfigurational quantum chemistry. *Proceedings of the National Academy of Science USA*, **104**, 4464–4469.

Fujimoto, K., Hayashi, S., Hasegawa, J., and Nakatsuji, H. 2007. Theoretical studies on the color-tuning mechanism in retinal proteins. *Journal of Chemical Theory and Computation*, **3**, 605–618.

Fujimoto, K., Hasegawa, J., and Nakatsuji, H. 2009. Color tuning mechanism of human red, green, and blue cone pigments: SAC-CI theoretical study. *Bulletin of the Chemical Society of Japan*, **82**, 1140–1148.

Fujimoto, K.J., Asai, K., and Hasegawa, J. 2010. Theoretical study of the opsin shift of deprotonated retinal Schiff base in the M state of bacteriorhodopsin. *Physical Chemistry Chemical Physics*, **12**, 13107–13116.

Gai, F., Hasson, K.C., McDonald, J.C., and Anfinrud, P.A. 1998. Chemical dynamics in proteins: the photoisomerization of retinal in bacteriorhodopsin. *Science*, **279**, 1886–1891.

González-Luque, R., Garavelli, G., Bernardi, F., Merchán, M., Robb, M.A., and Olivucci, M. 2000. Computational evidence in favor of a two-state, two-mode model of the retinal chromophore photoisomerization. *Proceedings of the National Academy of Science USA*, **97**, 9379–9384.

Groenhof, G., , Schäfer, L.V., Boggio-Pasqua, M., and Robb, M.A. 2009. *Handbook*

of Molecular Biophysics. Methods and Applications. Weinheim:Viley-VCH. Chap. Excited state dynamics in biomolecules, pages 93–134.

Hayashi, S., Tajkhorshid, E., Pebay-Peyroula, E., Royant, A., Landau, E.M., Navarro, J., and Schulten, K. 2001. Structural determinants of spectral tuning in retinal proteins - bacteriorhodopsin vs. sensory rhodopsin II. *Journal of Physical Chemistry B*, **105**, 10124–10131.

Hayashi, S., Tajkhorshid, E., and Schulten, K. 2003. Molecular dynamics simulation of bacteriorhodopsins photoisomerization using ab initio forces for the excited chromophore. *Biophysical Journal*, **85**, 1440.

Hayashi, S., Tajkhorshid, E., and Schulten, K. 2009. Photochemical reaction dynamics of the primary event of vision studied by means of a hybrid molecular simulation. *Biophysical Journal*, **96**, 403–416.

Hoffmann, M., Wanko, M., Strodel, P., König, P.H., Frauenheim, T., Schulten, K., Thiel, W., Tajkhorshid, E., and Elstner, M. 2006. Color tuning in rhodopsins: the mechanism for the spectral shift between bacteriorhodopsin and sensory rhodopsin II. *Journal of the American Chemical Society*, **128**, 10808–10818.

Hudson, B.S., Kohler, B.E., and Schulten, K. 1982. *Excited States*. Vol. 6. Academic Press, New York. Chap. Linear polyene electronic structure and potential surfaces, pages 1–95.

Khorana, H.G.J. 1992. Rhodopsin, photoreceptor of the rod cell. An emerging pattern for structure and function. *Journal of Biological Chemistry*, **267**, 1–4.

Kobayashi, T., Saito, T., and Ohtani, H. 2001. Real-time spectroscopy of transition states in bacteriorhodopsin during retinal isomerization. *Nature*, **414**, 531–534.

Kochendoerfer, G.G., and Mathies, R.A. 1996. Spontaneous emission study of the femtosecond isomerization dynamics of rhodopsin. *Journal of Physical Chemistry*, **100**, 14526–14532.

Kolber, Z.S., Dover, C.L. Van, Niederman, R.A., and Falkowski, P.G. 2000. Bacterial photosynthesis in surface waters of the open ocean. *Nature*, **407**, 177–179.

Koyama, Y., Kubo, K., Komori, M., Yasuda, H., and Mukai, Y. 1991. Effect of protonation on the isomerization properties of n-butylamine Schiff base of isomeric retinal as revealed by direct HPLC analyses: selection of isomerization pathways by retinal proteins. *Photochemistry and Photobiology*, **54**, 433–443.

Kukura, P., McCamant, D.W., Yoon, S., Wandschneider, D.B., and Mathies, R.A. 2005. Structural observation of the primary isomerization in vision with femtosecond-stimulated Raman. *Science*, **310**, 1006–1009.

Logunov, S.L., Sang, L., and El-Sayed, M.A. 1996. Excited state dynamics of a protonated retinal Schiff base in solution. *Journal of Physical Chemistry*, **100**, 18586–18591.

Nathans, J., Piantanida, T.P., Eddy, R.L., Shows, T.B., and Hogness, D.S. 1986. Molecular genetics of inherited variation in human color vision. *Science*, **232**, 203–210.

Polli, D., Altoé, P., Weingart, O., Spillane, K.M., Manzoni, C., Brida, D., Tomasello, G., Orlandi, G., Kukura, P., Mathies, R.A., Garavelli, M., and Cerullo, G. 2010. Conical intersection dynamics of the primary photoisomerization event in vision. *Nature*, **467**, 440–443.

Prokhorenko, V.I., Nagy, A.M., Waschuk, S.A., Brown, L.S., Birge, R.R., and Miller, R.J.D. 2006. Coherent control of retinal isomerization in bacteriorhodopsin. *Science*, **313**, 1257–1261.

Ren, L., Martin, C.M., Wise, K.J., Gillespie, N.B., Luecke, H., Lanyi, J.K., Spudich,

J.L., and Birge, R.R. 2001. Molecular mechanism of spectral tuning in sensory rhodopsin II. *Biochemistry*, **40**, 13906–13914.

Ritz, Th., Damjanovic, A., Schulten, K., Zhang, J.-P., and Koyama, Y. 2000. Efficient light harvesting through carotenoids. *Photosynthesis Research*, **66**, 125–144.

Ruhman, S., Hou, B., Friedman, N., Ottolenghi, M., and Sheves, M. 2002. Following evoluation of bacteriorhodopsin in its reactive excited state via stimulated emission pumping. *Journal of the American Chemical Society*, **124**, 8854–8858.

Salem, L. 1979. The sudden polarization effect and its possible role in vision. *Account of Chemical Research*, **119**, 12687–12688.

Sasaki, J., Brown, L.S., Chon, Y.-S., Kandori, H., Maeda, A., Needleman, R., and Lanyi, J.K. 1995. Conversion of bacteriorhodopsin into a chloride ion pump. *Science*, **269**, 73–75.

Scharf, B., and Engelhard, M. 1994. Blue halorhodopsin from natronobacterium pharaonis: wavelength regulation by anions. *Biochemistry*, **33**, 6387–6393.

Schoenlein, R. W., Peteanu, L.A., Mathies, R.A., and Shank, C.A. 1991. The first step in vision: femtosecond isomerization of rhodopsin. *Science*, **254**, 412–415.

Schulten, K., and Karplus, M. 1972. On the origin of a low-lying forbidden transition in polyenes and related molecules. *Chemical Physics Letters*, **14**, 305–309.

Schulten, K., and Tavan, P. 1978. A mechanism for the light-driven proton pump of Halobacterium halobium. *Nature*, **272**, 85–86.

Schulten, K., Dinur, U., and Honig, B. 1980. The spectra of carbonium ions, cyanine dyes, and protonated Schiff base polyenes. *Journal of Chemical Physics*, **73**, 3927–3935.

Shichida, Y., and Imai, H. 1998. Visual pigment: G-protein-coupled receptor for light signals. *Cellular and Molecular Life Science*, **54**, 1299–1315.

Shimono, K., Iwamoto, M., Sumi, M., and Kamo, N. 2000. Effects of three characteristic amino acid residues of pharaonis phoborhodopsin on the absorption maximum. *Photochemistry and Photobiology*, **72**, 141–5.

Spudich, J.L., and Jung, K.-H. 2005. *Hand Book of Photosensory Receptors*. Weinheim: Wiley-VCH. Chap. Microbial rhodopsins: Phylogenetic and functional diversity, pages 1–23.

Tavan, P., and Schulten, K. 1986. The low-lying excitations in long polyenes: A PPP-MRD-CI study. *Journal of Chemical Physics*, **85**, 6602–6609.

Tavan, P., and Schulten, K. 1987. Electronic excitations in finite and infinite polyenes. *Physical Review B*, **36**, 4337–4358.

Tully, J.C. 1990. Molecular dynamics with electronic transitions. *Journal of Chemical Physics*, **93**, 1061–71.

von Neumann, J., and Wigner, E.P. 1929. Concerning the behavior of eigenvalues in adiabatic processes. *Zeitschrift für Physik*, **30**, 467–470.

Wald, G. 1933. Vitamin A in the retina. *Nature*, **132**, 316–317.

Wang, Q., Schoenlein, R.W., Peteanu, L.A., Mathies, R.A., and Schank, C.V. 1994. Vibrationally coherent photochemistry in the femtosecond primary event of vision. *Science*, **266**, 422–424.

Wanko, M., Hoffmann, M., Strodel, P., Koslowski, A., Thiel, W., Neese, F., Frauenheim, T., and Elstner, M. 2005. Calculating absorption shifts for retinal proteins: computational challenges. *Journal of Physical Chemistry B*, **109**, 3606–3615.

Weiss, R.M., and Warshel, A. 1979. A new view of the dynamics of singlet cis-trans photoisomerization. *Journal of the American Chemical Society*, **101**, 6131–6133.

Zener, C. 1932. Non-adiabatic crossing of energy levels. *Proceedings of the Royal Society of London A*, **137**, 696–702.

Zhang, F., Aravanis, A.M., Adamantidis, A., de Lecea, L., and Deisseroth, K. 2007. Circuit-breakers: optical technologies for probing neural signals and systems. *Nature Reviews Neuroscience*, **8**, 205–218.